Graphene MEMS: AFM Probe Performance Improvement

Cristina Martin-Olmos,[†,‡] Haider Imad Rasool,[†,‡,§] Bruce H. Weiller,[⊥] and James K. Gimzewski[†,‡,§,*]

[†]Department of Chemistry and Biochemistry, University of California at Los Angeles, 607 Charles E. Young Drive East, Los Angeles, California 90095, United States, [‡]California NanoSystems Institute, 570 Westwood Plaza, Los Angeles, California 90095, United States, [§]WPI Center for Materials Nanoarchitectonics (MANA), National Institute for Materials Science (NIMS), 1-1 Namiki, Tsukuba, Ibaraki 305-0044, Japan, and [⊥]Micro/Nano Technology Department, Space Materials Laboratory, The Aerospace Corporation, Los Angeles, California 90009, United States

ABSTRACT We explore the feasibility of growing a continuous layer of graphene in prepatterned substrates, like an engineered silicon wafer, and we apply this as a mold for the fabrication of AFM probes. This fabrication method proves the fabrication of SU-8 devices coated with graphene in a full-wafer parallel technology and with high yield. It also demonstrates that graphene coating enhances the functionality of SU-8 probes, turning them conductive and more resistant to wear. Furthermore, it opens new experimental possibilities such as studying graphene–graphene interaction at the nanoscale with the precision of an AFM or the exploration of properties in nonplanar graphene layers.

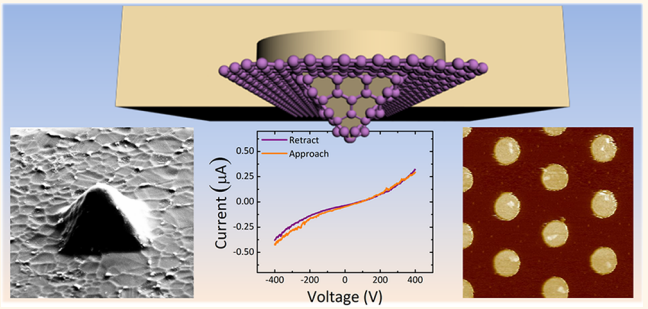

KEYWORDS: graphene · AFM · probes · MEMS · SU-8

Graphene has become one of the most influential discoveries of the last century. Since the initial experiments,[1,2] the amount of publications from academia and the industrial interest have been ever-growing. Most of the initial research on this material has been performed using devices obtained from mechanical exfoliation of monolayers from bulk graphite.[3] This has allowed extensive basic research in physics, chemistry, and materials science. In order to respond to the industrial interest in the material, different controlled methods for its production have been progressively appearing that aim to obtain devices and samples in a reliable, repeatable, and cost-effective manner for mass production. It is possible to summarize the methods to synthesize graphene in two domains, the bottom-up and the top-down approaches. The mechanical exfoliation is part of the top-down approach, which also includes the oxidation of graphite.[4] The main drawback of this approach is the difficulty of removing a single graphene sheet from the exfoliated layers and not being a scalable technique. The bottom-up approach involves the direct synthesis from carbon sources and can be scaled into a continuous process for mass production. The methods involved are based on a solid–gas phase deposition, such as chemical vapor deposition (CVD)[5] or plasma-enhanced CVD (PECVD),[6] or also graphitization of carbon-containing substrates, such as SiC.[7] It also embraces methods based in wet chemical reaction of ethanol and sodium followed by pyrolysis[8] or through organic synthesis.[9]

This tremendous international effort on the development of graphene growth methods has focused on flat substrates; direct growth of graphene layers on prepatterned substrates has remained elusive. We have shown[10,11] that graphene grows continuously over large areas on different copper terraces without the underlying substrate morphology affecting the atomic arrangement of the grown material. In this work, we apply the technique to grow graphene in prepatterned copper-coated substrates, and we apply this protocol for the fabrication of MEMS devices, in particular, AFM probes.[12]

Conformal deposition of graphene on prepatterned substrates opens a multitude of device fabrication possibilities. One of them is the addition of different layers to

* Address correspondence to gimzewski@cnsi.ucla.edu.

Received for review February 1, 2013 and accepted April 6, 2013.

Published online April 07, 2013
10.1021/nn400557b

the graphene, mostly by deposition, using the prepatterned substrate as a mold. This can result in hybrid 3D structures covered with graphene. In particular, a large variety of polymers could be spun on the substrate, like epoxy composites, which have already proven to be very versatile for different applications, including the fabrication of devices replicating Si molds. Epoxy-based resists provide cheap and fast fabrication processes, but their properties are not optimum when compared to solid-state materials. However, if the final devices are composed by a combination of a polymer and graphene, their mechanical, electrical, and functional properties might be improved substantially.[13] Such improvement has also been tackled with carbon nanotubes and nanoparticle dispersions in epoxy-based resists.[14,15] In this work, we report the fabrication of polymeric AFM probes covered by monolayer graphene that had been previously deposited on a prepatterned substrate. We also demonstrate how graphene improves the functionality of the probes by making them conductive and more resistant to wear.

RESULTS AND DISCUSSION

Fabrication of Graphene-Coated AFM Probes. We fabricate photoplastic probes following a similar process to the one presented elsewhere,[15,16] which is based on the multiple spin-coating, exposure, and development of SU-8 resist on a prepatterned silicon wafer, the latter being used as a mold for the tip. In our particular implementation, the substrate is prepared so that it has a continuous monolayer of CVD-grown graphene[17] (see Experimental Section).

Figure 1 summarizes the effectiveness of the graphene growth by showing a perfect coverage in edges and vertices of the patterned inverted pyramids (a) and (b). Figure 1c,d shows with further detail the continuity of the grown graphene in the smallest pattern (a 10 μm base sharp inverted pyramid). We can also observe an increase of the copper roughness after the growth. This is attributed to the high copper mobility at the growth temperature of 800 °C and that vacancies can become pinned between the graphene sheet and the copper during cooling.

Raman spectroscopy is performed on the prepatterned substrates coated with grown graphene in order to fully verify and assess the growth of single-layer graphene. Measurements are taken at different points on the substrate, including in the patterned cavities. Figure 2 shows a typical Raman spectrum (after the subtraction of the copper luminescent background) taken on the substrate after graphene growth. From the 2D/G peaks' intensity ratio and from the Lorentzian shape of the 2D peak, we conclude that we have a continuous graphene monolayer all across the wafer. This shows the major strengths of this

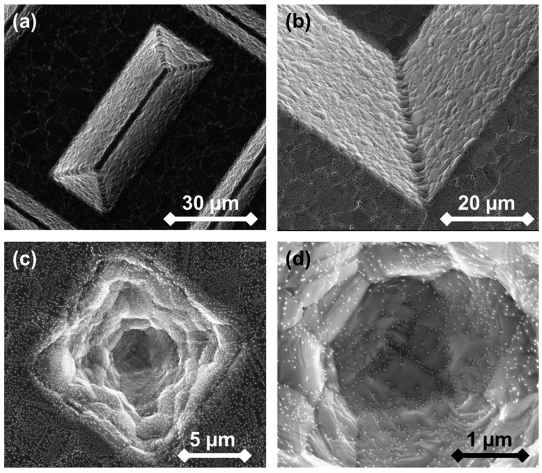

Figure 1. Graphene layer deposition. SEM micrographs of structures that have been KOH etched in Si, with 300 nm of growth SiO_2, 500 nm of deposited Cu, and growth graphene on top. (a) Etched rectangle and (b) zoom in of the vertexes of the rectangle to show the continuity of the growth graphene in the patterned substrate. (c) Inverted pyramid used to mold the tip for an AFM probe. (d) Zoom in of the apex of the pyramid to show the continuity of the graphene at the bottom.

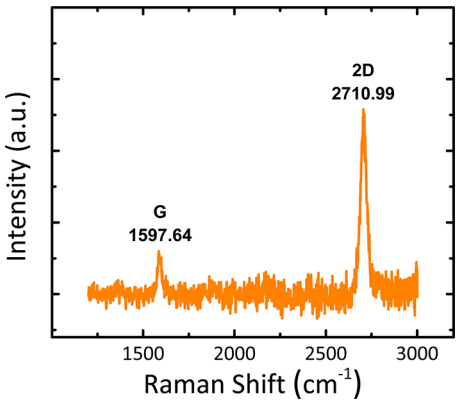

Figure 2. Characterization of as-grown graphene. Raman spectrum of graphene on a prepatterned Si substrate with thermally grown SiO_2 and coated with copper (after subtraction of copper luminescent background). From the 2D/G peaks' intensity ratio and from the Lorentzian shape of the 2D peak, we conclude that we have a continuous graphene monolayer all across the wafer.

method to grow graphene: its remarkable high yield, reliability, and layer continuity and conformity. It overcomes, for example, the fragility and uncertainties of the deposition of mechanically exfoliated graphene on either substrates or devices.

Once the substrates are patterned to create the tip molds by using KOH, then a 300 nm layer of thermal SiO_2 is grown and a 500 nm layer of Cu is deposited by evaporation (Figure 3, step 1, Experimental Section). This copper layer is subsequently used as a seed layer for graphene growth. The high temperatures of such a process might cause Cu to sublime and even form islands on the patterned substrate if the layer is too thin. Thus, the copper layer thickness is chosen to

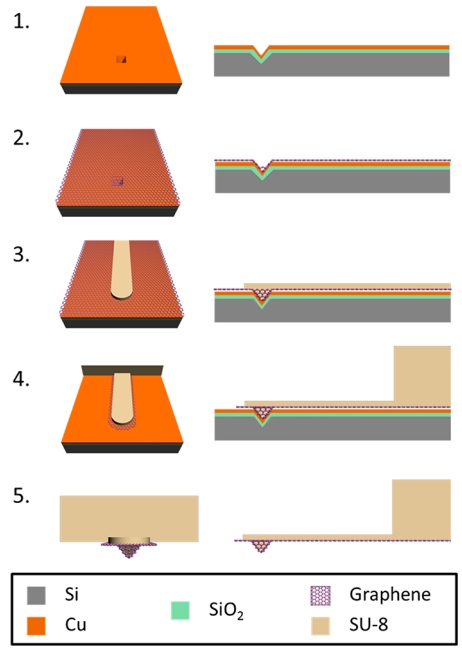

Figure 3. Fabrication process scheme. The fabrication process of photoplastic probes was based on the multiple spin-coating, exposure, and development of SU-8 on a prestructured mold. Step 1 consists of preparing the silicon wafer by selectively etching the tip with KOH, growing a thermal silicon oxide, and finally coating the surface with copper. Step 2 is the CVD growth of a continuous layer of graphene due to the copper coating. During step 3, a thin layer of SU-8 is spin-coated, exposed, and developed in order to fill the tip mold and define the cantilever. Step 4 comprises an argon dry etch to remove the graphene elsewhere that is not already protected by SU-8. Also, a second and thicker layer of SU-8 is processed in order to shape the body of the probe. Finally, during step 5, the AFM probe is released without damaging the graphene layer by etching the silicon oxide with HF, the silicon with KOH, and the Cu with a commercially available Cu etchant solution. Probes are rinsed three times in DI water.

ensure a continuous layer of graphene. We expect that annealing at higher pressures and optimizing growth conditions will allow decreasing the amount of Cu deposited, which will lead to better AFM tip geometries.

After graphene growth (Figure 3, step 2), substrates are dehydrated, and the first layer of SU-8 is deposited (around 10 μm thick). The copper layer is prevented from oxidation during dehydration due to the graphene coverage.[18] The SU-8 layer is pr-ebaked, exposed, post-baked, and developed to transfer the cantilever shape design (Figure 3, step 3). In order to improve adhesion of subsequent layers and to help in the final (release) step, an Ar plasma etch is performed to remove the graphene not protected by the patterned SU-8 layer (Figure 3, step 4). Evidence of graphene removal is seen when dehydrating the substrates prior to the second SU-8 layer deposition, and we observe oxidation of copper at the zones where graphene is not present. The second and thicker layer of SU-8 (200 μm thick) is patterned to transfer the

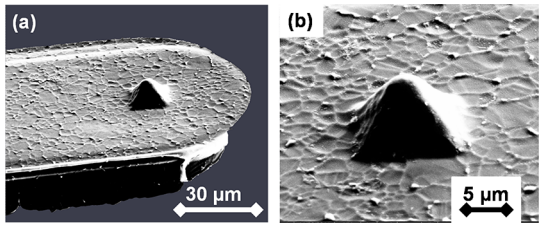

Figure 4. Fabricated graphene-coated SU-8 AFM probes. SEM Micrographs: (a) released SU-8 AFM probe coated with graphene (background has been colored for improved contrast). (b) Zoom in of the tip showing again the continuity of the graphene and the dullness.

chip body with similar dimensions and shape to commercially available cantilever chip designs (Figure 3, step 4). The thickness of this second layer is chosen to make the chips robust to manual handling with tweezers. Finally, the probes are released from the substrate (Figure 3, step 5) by etching the whole silicon substrates in KOH and subsequently removing the copper layer in a copper etchant solution. This process has a fair yield and causes little damaging to the graphene layer.

A variety of cantilever dimensions are included within the fabricated designs. Lengths ranged from 250 to 750 μm, widths of 40 $\pm$ 3 μm, and thickness of 12.5 $\pm$ 0.5 μm (measured with a profiler). Fabrication yield for this process is higher than 80%, and all cantilevers present very low stress and stress gradient as a result of the hard bake step performed before developing in a N_2-rich environment.[19] Low stress gradient is inferred from the fact that static curvature and deflection of the cantilevers is very small which, in turn, makes the acquisition of AFM images very straightforward because of an easy laser alignment. Low intrinsic stress is inferred from a visual inspection of the thick SU-8 layer, which does not show cracks or distortions on its surface.[20]

From the SEM images taken of the fabricated AFM probes (Figure 4), it is possible to see that the cross section of our cantilevers is not purely rectangular. This is a known effect when performing SU-8 lithography on highly reflective surfaces. For bigger mechanical structures, it does not have any influence in their behavior.[21] In our case, even though the structures are smaller, it has an insignificant influence on the resonance frequency[22,23] as we analyze later in the text. Figure 4 also shows that the graphene layer nicely covers the whole surface of the SU-8 body and cantilever. By zooming in on the tip (Figure 4b), it can be seen that the graphene complies perfectly with the smooth edges of the SU-8 pyramid. Also, the tip shows a rather dull vertex that can decrease the resolution of the probes' performance in applications where the substrate has high aspect ratio features. This loss of sharpness is attributed to the 500 nm layer of copper, required to grow continuous graphene on

the substrate, which renders a blunt mold for the tip fabrication. As mentioned before, this is expected to be solved in the near future *via* optimization of the graphene deposition conditions, which will allow for thinner Cu layers (*i.e.*, sharper tips). Nevertheless, there exist several applications for AFM probes where sharp tips are not necessary. AFM indentation, friction, adhesion, magnetic interaction, and conductive measurements can benefit from an increased contact area between substrate and tip. In addition, a well-known tip radius of curvature is preferred over sharp tips in mechanical studies with AFM spectroscopy on soft biological materials.[24]

In order to evaluate the properties of these fabricated graphene-coated probes, uncoated SU-8 probes are fabricated as a reference using the exact same process but skipping the CVD deposition. Therefore, not only the cantilever mechanical properties (spring constant and resonant frequency) but also the final tip radius of both coated and uncoated SU-8 probes are directly comparable.

AFM Probe Characterization. Probes are tested using a commercial Bruker Dimension Icon scanning probe microscope (SPM). All of the chips perfectly fit in commercial AFM holders, and good reflection of the instrumentation deflection laser is easily obtained due to the low initial deflection that the fabricated probes have.

Resonance frequency and quality factor are measured for all cantilevers used in the experiments. Resonance frequency values range from 4 to 65 kHz, and they show, for given cantilever dimensions, a variability of approximately $\pm$10%. This is mostly caused by variations in the fabrication process flow, for example, the measured variability in thickness of the SU-8 layer defining the cantilevers. The values can be estimated analytically within a variability assuming a rectangular cantilever cross section and the reported material properties for SU-8 (render insignificant the side effects of the reflective surface on the cantilever shape).[25] As a consequence of these variations, it is not possible to appreciate a difference between graphene-coated and bare SU-8 probes. Graphene Young's modulus is reported to be 1.0 TPa,[26] indeed, the largest for any known material. In addition, intrinsic stress in graphene has been reported to reach very high values ($\geq$1 GPa). The combination of these two effects causes an increase of up to about 3% in the resonance frequency,[27,28] which is smaller than the mentioned dispersion in the cantilevers frequency, and therefore, it is not possible to differentiate the graphene-coated probes from those that are not. The quality factors do not offer also any significant differentiation, all of them being 35 $\pm$ 5, which means that the damping is still dominated by internal dissipation within the polymer.

Both tapping mode and contact mode imaging are performed with the probes. Figure 5 shows typical scans of the same calibration sample, using both graphene-coated probes and reference (bare SU-8) probes, in tapping and contact mode. It can be seen from the figure that both tapping and contact mode images have enough resolution to fully resolve the features in our calibration sample, which consists of 800 nm diameter and 40 nm thick Ag pillars on a SiO_2 substrate. One of the major challenges that SU-8 AFM probes present is the preservation of tip sharpness.[16,29] Polymeric AFM probes are usually operated in tapping mode because in contact mode they wear very easily due to the low hardness of the material, and even then, they need to be replaced rather often. SU-8 hardness is $\sim$0.43 GPa,[30] while Si is $\sim$11.90 GPa,[31] which explains that when SU-8 is slightly pressed against studded silicon surfaces, the tip is deformed and easily worn out. As a practical consequence, it is very difficult to finish a full first scan with such probes in contact mode, as it is clearly shown in Figure 5b. On the other hand, the graphene-coated SU-8 AFM probes remained invariable with the same resolution for many scans (Figure 5c), even when the scan size was increased. It is unclear at the moment whether this improvement is due to the increase in hardness or due to a reduction in the adhesion forces between the tip and sample. A thorough investigation is necessary to quantify tip degradation over time.[32,33] This cannot be done using traditional methods as SEM imaging because SU-8 rapidly charges, making high precision imaging difficult. In any case, it has been shown repeatedly that carbon probes present less degradation. This is true for monolithic diamond probes,[34] for diamond-coated probes,[35] or for carbon-coated[36] probes. In the latter case, for example, carbon coating on flared Si probes improves their lifetime 15 times. In our work, the tips' lifetime with the graphene layer is substantially improved, but comparison to any commercially available contact mode AFM probes is not fair at the moment, given our tips large original radius.

Conductivity of the graphene layer is also tested by performing *I*–*V* curves on a biased Pt substrate. Figure 6 shows exemplary curves performed with a bare SU-8 AFM probe (Figure 6a), with a graphene-coated probe (Figure 6b) and with a Pt-coated silicon probe (Figure 6c). SU-8 is well-known for its insulating properties,[37] and as expected, no conduction can be measured at any voltage. Platinum on the other hand has an excellent conductivity, so the measurement with the AFM rapidly saturated the preamplifier measurement range. Graphene-coated SU-8 probes show a conductive behavior, proving the continuity of the layer on the AFM probe. In addition, the *I*–*V* curves show a nonlinear behavior with a smaller slope close

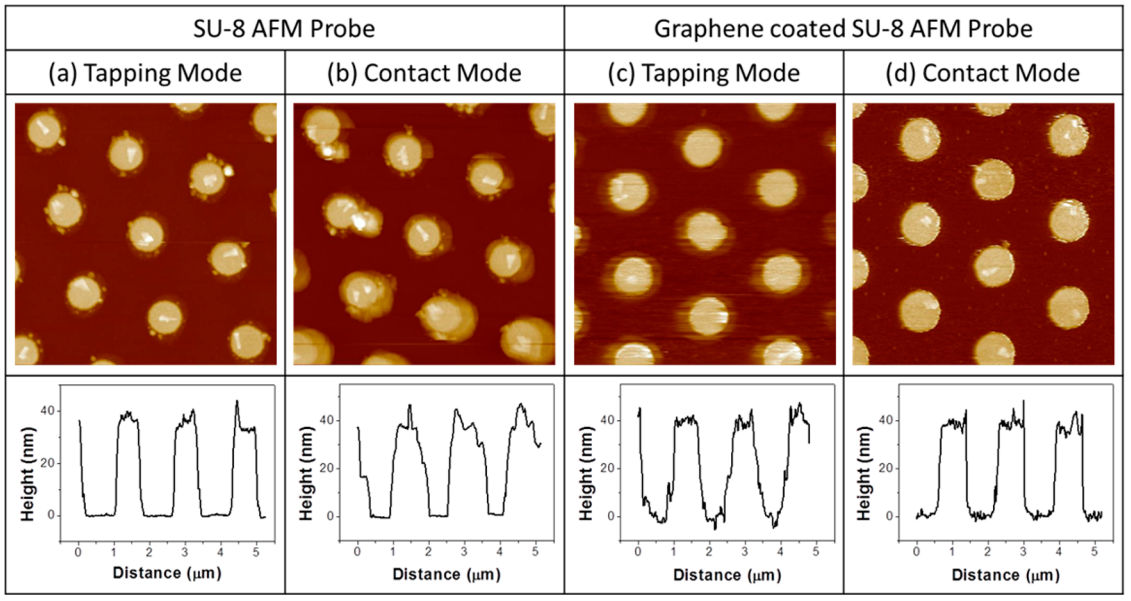

Figure 5. Lifetime and resolution of the fabricated probes. SU-8 probes and graphene-coated SU-8 probes were fabricated using the same process steps and tested on a SiO_2 substrate with 800 nm diameter pillars of Ag deposited through stencil lithography. (a) Tapping mode image and profile of a SU-8 probe without graphene and showing good resolution. (b) Contact mode image and profile of the same SU-8 probe without graphene showing the loss of resolution due to SU-8 softness and fast wear of the tip. (c) Tapping mode image and profile of a graphene-coated AFM probe showing a 10% loss of resolution compared to the noncoated one. (d) Contact mode image and profile of the same graphene-coated AFM probe showing an increased strength to wear and a longer lifetime.

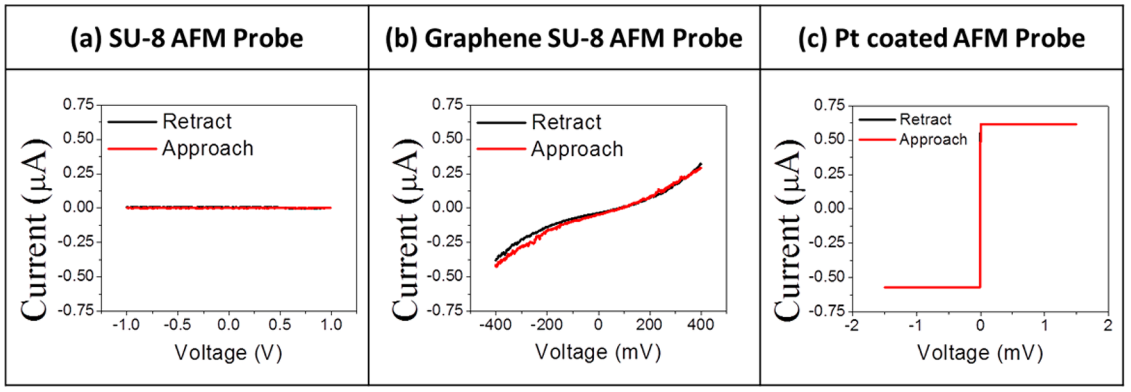

Figure 6. Conductivity in AFM probes. A SU-8 probe (a), a graphene-coated SU-8 probe (b), and a Pt-coated Si commercial probe (c) were tested using contact mode and connected to a preamplifier to measure the current while sweeping the voltage in a Pt-coated substrate. Resulting *I*−*V* curves show a dielectric behavior for SU-8 probes (a), a semiconductor behavior for graphene-coated SU-8 probes (b), and a high conductive behavior for Pt-coated Si probes (c).

to 0 V, which is characteristically found in other contact experiments with graphene.[38]

Providing SU-8 structures with conductivity is a long-standing challenge in the SU-8 MEMS community. In most cases, the approach has been based on doping the polymer to turn it conductive, that is, incorporating conductive compounds into the polymer bulk.[39] However, such efforts have not been entirely successful.[40,41] The other option consists of covering the polymer with thin conductive layers, mostly metals.[42] Our approach is the ultimate limit for this second option, given that graphene is the thinnest conductive layer and has important implications for sensors and actuators.[43] In addition, graphene also improves the reliability and durability of the structures.

CONCLUSIONS

Graphene-coated polymer MEMS have been fabricated after the development of the process to grow continuous graphene on prepatterned Si substrates. The fabrication steps utilized in the process are very standard and highly compatible with current Si fabrication technology, which allows its application in any clean room or microtechnology laboratory. The fabricated conductive graphene-coated AFM probes have proven to present improved endurance, operational stability, and large shelf life, which are crucial

parameters for practical applications. Even though sharper tips need to be produced for these probes to be fully functional in any scanning experiment, they can be useful for some experiments as indentation on biological material.[44,45] In addition, this kind of device introduces the possibility of probing graphene properties by also using graphene. Until now, most of the experiments involving graphene are biased by the interactions of graphene with other materials. Graphene-coated AFM probes would allow studies on friction, adhesion, conductivity, *etc.* using graphene as a probing material and down at the nanoscale.

EXPERIMENTAL SECTION

Substrate Preparation. Prepatterned substrates for AFM probes are prepared by using standard microfabrication steps. The starting point is 100 mm silicon wafers with a 100 nm thick layer of thermally grown SiO_2. This layer is patterned using lithography and dry etching to define circles of different diameters. After immersion in a potassium hydroxide solution (40 % KOH in weight at 60 °C) for 10 min, inverted pyramids are defined, which are eventually used as a mold for the AFM tips. A thin layer of thermal SiO_2 is grown to serve as a sacrificial layer, and subsequently, the patterned substrates are coated with 500 nm thick evaporated high-purity copper (>99.999%). Finally, the wafer is cleaved into small chips before performing graphene growth.

Graphene Growth. Graphene is grown by chemical vapor deposition (CVD) in a tube furnace, following the method started by Ruoff[17] and that we already used in the past.[10] Wafer pieces are inserted into a 2 in. quartz tube and heated up to 800 °C under a hydrogen flow of 5 sccm in the tube furnace. Once the growth temperature was reached and stabilized, methane (CH_4) was flowed for 15 min as the carbon source for growth at a flow rate of 35 sccm. The overall growth pressure during growth was set to 7.5 Torr and maintained with an electronically controlled gate valve.

AFM Probe Fabrication. Before each lithography step, substrates are dehydrated by placing them on a hot plate at 150 °C for 2 min. SU-8 is then deposited by spin coating at 2000 rpm of SU-8-2010 for the thinner layer (10 μm) defining the cantilevers and at 800 rpm of SU-8-2100 for the thicker layer (200 μm) defining the chip body. A soft bake is performed at 90 °C during 15 min for the thinner layer and during 2 h for the thicker layer. Then the layers are locally exposed using a dose of 410 μJ/cm^2 (200 μm) or a dose of 145 μJ/cm^2 (10 μm). A hard bake is performed prior to development, which consist of baking the samples in a hot plate at 120 °C for 2 h in a rich environment of N_2. Development is performed in PGMEA (propylene glycol monomethyl ether acetate) for different times depending of the layer thickness. Graphene is etched after development of the first SU-8 layer using an argon plasma (50 sccm Ar, 50 mTorr pressure, 78 W forward power) for 1 min.

Final release of the probes is performed in three steps. The substrates were first dipped in buffered oxide etch (solution 6:1 HF/NH_4OH) for 30 min, to remove the SiO_2 on the backside of the wafer. After a thorough rinse in DI water, they were immersed in KOH (20% concentration at 60 °C) for 5−10 h, until the SU-8 was floating, completely detached from the silicon mold. The SU-8 devices were rinsed in DI water and dipped in a commercially available Cu etchant solution (a concentrated solution of 25−35% $FeCl_3$ and 3−4% HCl) for 5 min to completely guarantee the full removal of Cu. Finally, the chips were rinsed three times in three different beakers containing DI water.

AFM Experiments. AFM experiments are done using a commercial Bruker Dimension Icon scanning probe microscope (SPM). Tapping and contact mode measurements are performed on a calibration sample that is a SiO_2 substrate with 800 nm diameter pillars of Ag deposited through stencil lithography. Scans are 5 × 5 μm in size and are performed at a scan rate of 1 Hz. Scans consist in 512 lines with 512 samples/line.

Conductive AFM measurements are performed applying a voltage between the tip and the substrate. The *I*−*V* curve is measured with a commercially available current amplifier (*I*/*V* converter).

Conflict of Interest: The authors declare no competing financial interest.

Acknowledgment. This work has been partially financially supported by the EC through the Marie Curie Grant "SCANCER" PIOF-2008-237800. The authors are very thankful to the Nanoelectronics Research Facility and the Integrated Systems Nanofabrication Cleanroom at the University of California Los Angeles for their support during device fabrication; and to the Nano and Pico Characterization Lab at the California NanoSystems Institute for their support during device characterization.

REFERENCES AND NOTES

1. Geim, A. K.; Novoselov, K. S. The Rise of Graphene. *Nat. Mater.* **2007**, *6*, 183–191.
2. Novoselov, K. S.; Geim, A. K.; Morozov, S. V.; Jiang, D.; Zhang, Y.; Dubonos, S. V.; Grigorieva, I. V.; Firsov, A. A. Electric Field Effect in Atomically Thin Carbon Films. *Science* **2004**, *306*, 666–669.
3. Bunch, J. S.; van der Zande, A. M.; Verbridge, S. S.; Frank, I. W.; Tanenbaum, D. M.; Parpia, J. M.; Craighead, H. G.; McEuen, P. L. Electromechanical Resonators from Graphene Sheets. *Science* **2007**, *315*, 490–493.
4. Becerril, H. A.; Mao, J.; Liu, Z.; Stoltenberg, R. M.; Bao, Z.; Chen, Y. Evaluation of Solution-Processed Reduced Graphene Oxide Films as Transparent Conductors. *ACS Nano* **2008**, *2*, 463–470.
5. Chen, Z. P.; Ren, W. C.; Gao, L. B.; Liu, B. L.; Pei, S. F.; Cheng, H. M. Three-Dimensional Flexible and Conductive Interconnected Graphene Networks Grown by Chemical Vapour Deposition. *Nat. Mater.* **2011**, *10*, 424–428.
6. Wang, Y.; Xu, X. F.; Lu, J.; Lin, M.; Bao, Q. L.; Ozyilmaz, B.; Loh, K. P. Toward High Throughput Interconvertible Graphane-to-Graphene Growth and Patterning. *ACS Nano* **2010**, *4*, 6146–6152.
7. Emtsev, K. V.; Bostwick, A.; Horn, K.; Jobst, J.; Kellogg, G. L.; Ley, L.; McChesney, J. L.; Ohta, T.; Reshanov, S. A.; Rohrl, J.; *et al.* Towards Wafer-Size Graphene Layers by Atmospheric Pressure Graphitization of Silicon Carbide. *Nat. Mater.* **2009**, *8*, 203–207.
8. Choucair, M.; Thordarson, P.; Stride, J. A. Gram-Scale Production of Graphene Based on Solvothermal Synthesis and Sonication. *Nat. Nanotechnol.* **2009**, *4*, 30–33.
9. Wang, X.; Zhi, L. J.; Tsao, N.; Tomovic, Z.; Li, J. L.; Mullen, K. Transparent Carbon Films as Electrodes in Organic Solar Cells. *Angew. Chem., Int. Ed.* **2008**, *47*, 2990–2992.
10. Rasool, H. I.; Song, E. B.; Allen, M. J.; Wassei, J. K.; Kaner, R. B.; Wang, K. L.; Weiller, B. H.; Gimzewski, J. K. Continuity of Graphene on Polycrystalline Copper. *Nano Lett.* **2011**, *11*, 251–256.
11. Rasool, H. I.; Song, E. B.; Mecklenburg, M.; Regan, B. C.; Wang, K. L.; Weiller, B. H.; Gimzewski, J. K. Atomic-Scale Characterization of Graphene Grown on Copper (100) Single Crystals. *J. Am. Chem. Soc.* **2011**, *133*, 12536–12543.
12. Villanueva, G.; Plaza, J. A.; Sanchez, A.; Zinoviev, K.; Perez-Murano, F.; Bausells, J. DRIE Based Novel Technique for AFM Probes Fabrication. *Microelectron. Eng.* **2007**, *84*, 1132–1135.
13. Huang, X.; Qi, X. Y.; Boey, F.; Zhang, H. Graphene-Based Composites. *Chem. Soc. Rev.* **2012**, *41*, 666–686.

14. Lu, S. X.; Panchapakesan, B. Optically Driven Nanotube Actuators. *Nanotechnology* **2005**, *16*, 2548–2554.
15. Ingrosso, C.; Martin-Olmos, C.; Llobera, A.; Innocenti, C.; Sangregorio, C.; Striccoli, M.; Agostiano, A.; Voigt, A.; Gruetzner, G.; Brugger, J.; *et al.* Oxide Nanocrystal Based Nanocomposites for Fabricating Photoplastic AFM Probes. *Nanoscale* **2011**, *3*, 4632–4639.
16. Genolet, G.; Brugger, J.; Despont, M.; Drechsler, U.; Vettiger, P.; de Rooij, N. F.; Anselmetti, D. Soft, Entirely Photoplastic Probes for Scanning Force Microscopy. *Rev. Sci. Instrum.* **1999**, *70*, 2398–2401.
17. Li, X. S.; Cai, W. W.; An, J. H.; Kim, S.; Nah, J.; Yang, D. X.; Piner, R.; Velamakanni, A.; Jung, I.; Tutuc, E.; *et al.* Large-Area Synthesis of High-Quality and Uniform Graphene Films on Copper Foils. *Science* **2009**, *324*, 1312–1314.
18. Chen, S. S.; Brown, L.; Levendorf, M.; Cai, W. W.; Ju, S. Y.; Edgeworth, J.; Li, X. S.; Magnuson, C. W.; Velamakanni, A.; Piner, R. D.; *et al.* Oxidation Resistance of Graphene-Coated Cu and Cu/Ni Alloy. *ACS Nano* **2011**, *5*, 1321–1327.
19. Martin, C.; Llobera, A.; Villanueva, G.; Voigt, A.; Gruetzner, G.; Brugger, J.; Perez-Murano, F. Stress and Aging Minimization in Photoplastic AFM Probes. *Microelectron. Eng.* **2009**, *86*, 1226–1229.
20. Li, B.; Liu, M.; Chen, Q. F. Low-Stress Ultra-Thick SU-8 UV Photolithography Process for MEMS. *J. Micro/Nanolith. MEMS MOEMS* **2005**, *4*, 043008.
21. Llobera, A.; Villanueva, G.; Cadarso, V. J.; Büttgenbach, S.; Plaza, J. A. Polymeric MOEMS Variable Optical Attenuator. *IEEE Photonics Technol. Lett.* **2006**, *18*, 2425–2427.
22. Sadewasser, S.; Villanueva, G.; Plaza, J. A. Special Cantilever Geometry for the Access of Higher Oscillation Modes in Atomic Force Microscopy. *Appl. Phys. Lett.* **2006**, *89*, 033106.
23. Villanueva, L. G.; Karabalin, R. B.; Matheny, M. H.; Chi, D.; Sader, J. E.; Roukes, M. L. Nonlinearity in Nanomechanical Cantilevers. *Phys. Rev. B* **2013**, *87*, 024304.
24. Rico, F.; Roca-Cusachs, P.; Gavara, N.; Farre, R.; Rotger, M.; Navajas, D. Probing Mechanical Properties of Living Cells by Atomic Force Microscopy with Blunted Pyramidal Cantilever Tips. *Phys. Rev. E* **2005**, *72*, 021914.
25. Hopcroft, M.; Kramer, T.; Kim, G.; Takashima, K.; Higo, Y.; Moore, D.; Brugger, J. Micromechanical Testing of SU-8 Cantilevers. *Fatigue Fract. Eng. Mater. Struct.* **2005**, *28*, 735–742.
26. Lee, C.; Wei, X. D.; Kysar, J. W.; Hone, J. Measurement of the Elastic Properties and Intrinsic Strength of Monolayer Graphene. *Science* **2008**, *321*, 385–388.
27. Karabalin, R. B.; Villanueva, L. G.; Matheny, M. H.; Sader, J. E.; Roukes, M. L. Stress-Induced Variations in the Stiffness of Micro- and Nanocantilever Beams. *Phys. Rev. Lett.* **2012**, *108*, 236101.
28. Timoshenko, S.; Goodier, J. N. *Theory of Elasticity*, 3rd ed.; McGraw-Hill: New York, 1969; p 567.
29. Genolet, G.; Despont, M.; Vettiger, P.; Anselmetti, D.; de Rooij, N. F. All-Photoplastic, Soft Cantilever Cassette Probe for Scanning Force Microscopy. *J. Vac. Sci. Technol., B* **2000**, *18*, 617–620.
30. Al-Halhouji, A. T.; Kampen, I.; Krah, T.; Büttgenbach, S. Nanoindentation Testing of SU-8 Photoresist Mechanical Properties. *Microelectron. Eng.* **2008**, *85*, 942–944.
31. Bhushan, B.; Li, X. D. Micromechanical and Tribological Characterization of Doped Single-Crystal Silicon and Polysilicon Films for Microelectromechanical Systems Devices. *J. Mater. Res.* **1997**, *12*, 54–63.
32. Gotsmann, B.; Lantz, M. A. Atomistic Wear in a Single Asperity Sliding Contact. *Phys. Rev. Lett.* **2008**, *101*, 125501.
33. Liu, J. J.; Notbohm, J. K.; Carpick, R. W.; Turner, K. T. Method for Characterizing Nanoscale Wear of Atomic Force Microscope Tips. *ACS Nano* **2010**, *4*, 3763–3772.
34. Liu, J.; Grierson, D. S.; Moldovan, N.; Notbohm, J.; Li, S.; Jaroenapibal, P.; O'Connor, S. D.; Sumant, A. V.; Neelakantan, N.; Carlisle, J. A.; *et al.* Preventing Nanoscale Wear of Atomic Force Microscopy Tips through the Use of Monolithic Ultrananocrystalline Diamond Probes. *Small* **2010**, *6*, 1140–1149.
35. Bhaskaran, H.; Gotsmann, B.; Sebastian, A.; Drechsler, U.; Lantz, M. A.; Despont, M.; Jaroenapibal, P.; Carpick, R. W.; Chen, Y.; Sridharan, K. Ultralow Nanoscale Wear through Atom-by-Atom Attrition in Silicon-Containing Diamond-like Carbon. *Nat. Nanotechnol.* **2010**, *5*, 181–185.
36. Liu, H.; Klonowski, M.; Kneeburg, D.; Dahlen, G.; Osborn, M.; Bao, T. Advanced Atomic Force Microscopy Probes: Wear Resistant Designs. *J. Vac. Sci. Technol. B* **2005**, *23*, 3090–3093.
37. Martin-Olmos, C.; Villanueva, L. G.; van der Wal, P. D.; Llobera, A.; de Rooij, N. F.; Brugger, J.; Perez-Murano, F. Conductivity of SU-8 Thin Films through Atomic Force Microscopy Nano-Patterning. *Adv. Funct. Mater.* **2012**, *22*, 1482–1488.
38. Hauquier, F.; Alamarguy, D.; Viel, P.; Noel, S.; Filoramo, A.; Huc, V.; Houze, F.; Palacin, S. Conductive-Probe AFM Characterization of Graphene Sheets Bonded to Gold Surfaces. *Appl. Surf. Sci.* **2012**, *258*, 2920–2926.
39. Voigt, A.; Heinrich, M.; Martin, C.; Llobera, A.; Gruetzner, G.; Perez-Murano, F. Improved Properties of Epoxy Nanocomposites for Specific Applications in the Field of MEMS/NEMS. *Microelectron. Eng.* **2007**, *84*, 1075–1079.
40. Gammelgaard, L.; Rasmussen, P. A.; Calleja, M.; Vettiger, P.; Boisen, A. Microfabricated Photoplastic Cantilever with Integrated Photoplastic/Carbon Based Piezoresistive Strain Sensor. *Appl. Phys. Lett.* **2006**, *88*, 113508.
41. Martin-Olmos, C.; Villanueva, L. G.; Llobera, A.; Voigt, A.; Gruetzner, G.; Abadal, G.; Perez-Murano, F. Opto-Thermal Actuation in Double Layer Polymer Microcantilevers. In *Nano-Opto-Mechanical Systems*; Esteve, J., Terentjev, E. M., Campo, E. M., Eds.; SPIE: Bellingham, WA, 2011; Vol. 8107, p 81070.
42. Johansson, A.; Janting, J.; Schultz, P.; Hoppe, K.; Hansen, I. N.; Boisen, A. SU-8 Cantilever Chip Interconnection. *J. Micromech. Microeng.* **2006**, *16*, 314–319.
43. Zhu, S.-E.; Shabani, R.; Rho, J.; Kim, Y.; Hong, B. H.; Ahn, J.-H.; Cho, H. J. Graphene-Based Bimorph Microactuators. *Nano Lett.* **2011**, *11*, 977–981.
44. Plodinec, M.; Loparic, M.; Monnier, C. A.; Obermann, E. C.; Zanetti-Dallenbach, R.; Oertle, P.; Hyotyla, J. T.; Aebi, U.; Bentires-Alj, M.; LimRoderick, Y. H.; *et al.* The Nanomechanical Signature of Breast Cancer. *Nat. Nanotechnol.* **2012**, *7*, 757–765.
45. Cross, S. E.; Jin, Y.-S.; Rao, J.; Gimzewski, J. K. Nanomechanical Analysis of Cells from Cancer Patients. *Nat. Nanotechnol.* **2007**, *2*, 780–783.